Sensors and Materials, Vol. 30, No. 8 (2018) 1841–1852
MYU Tokyo

S & M 1641

Automatic Detection of Dense Calcium and Acoustic Shadow in Intravascular Ultrasound Images by Dual-threshold-based Segmentation Approach

Ju Hwan Lee,[1] Ga Young Kim,[2] Yoo Na Hwang,[2] and Sung Min Kim[1,2*]

[1]Department of Medical Devices Industry, Dongguk University-Seoul,
(04620) 30, Pildong-ro 1-gil, Jung-gu, Seoul, Republic of Korea
[2]Department of Medical Biotechnology, Dongguk University-Bio Medi Campus,
(10326) 32, Dongguk-ro, Ilsandong-gu, Goyang-si, Gyeonggi-do, Republic of Korea

(Received May 15,2017; accepted March 15, 2018)

Keywords: intravascular ultrasound, virtual histology, dense calcium, acoustic shadow, dual threshold

The purpose of this study was to automatically detect dense calcium (DC) and acoustic shadow regions in intravascular ultrasound (IVUS) images by a dual-threshold-based segmentation approach. Three hundred grayscale IVUS and corresponding virtual histology (VH)-IVUS images of human coronary arteries were obtained using a 20 MHz commercial catheter. Plaque regions between intima and media-adventitial borders were manually extracted from all IVUS images. To detect DC and acoustic shadow regions automatically, DC candidates were first selected from plaque regions on the basis of intensity. The shadow mask of each DC candidate was then obtained by calculating its centroid. A DC candidate involving acoustic shadow was finally selected as DC tissue. The segmentation performance of the proposed approach was quantitatively evaluated using the area difference, DC ratio, Hausdorff distance, and Dice similarity coefficient. Quantitative results indicated that all the parameters for the proposed approach were highly similar to those of VH-IVUS. Despite the relatively low agreement (64.1%) for the DC tissue, reliable performance was found for the proposed approach. These experimental results suggest that the proposed method has clinical applicability for diagnosing cardiovascular diseases in IVUS images.

1. Introduction

Atherosclerosis is an inflammatory fibroproliferative disease characterized by deposits in the arterial vessel wall over time.(1) These atherosclerotic plaques are composed of lipids, inflammatory cells, and calcium deposits.(2,3) The disruption of an atherosclerotic plaque is the most critical cause of cardiovascular diseases, including angina, myocardial infarction, and sudden cardiac death.(4) Therefore, the early diagnosis and accurate assessment of plaque composition are imperative. They can allow clinicians to choose appropriate pharmaceutical or interventional therapies. In addition, plaque characterization could provide beneficial

*Corresponding author: e-mail: smkim@dongguk.edu
https://dx.doi.org/10.18494/SAM.2018.1905

ISSN 0914-4935

information for longitudinal studies of atherosclerosis or for understanding the process of vascular remodeling.[5]

Over the last decade, several imaging techniques have been developed to visualize the arterial lumen and wall. Among these techniques, intravascular ultrasound (IVUS) is the most widely used diagnostic tool. It provides a two-dimensional view of the arterial wall and allows thorough visualization of the plaque.[6,7] Using a specially designed catheter, IVUS not only provides real-time cross-sectional images of the coronary lumen and wall, but also introduces morphological information such as plaque shape and size.[8,9] Virtual histology (VH) is a new technique that characterizes arterial plaque based on the radio frequency (RF) signal analysis of reflected ultrasound pulses.[10,11] VH-IVUS can identify the media and four components of plaque [fibrous tissue (FT), fibro-fatty tissue (FFT), necrotic core (NC), and calcified tissue (DC)] with a color-coded map.[10,11] With a VH-IVUS image, clinicians can realize a more accurate characterization of plaque composition. Although the RF signal provides additional information compared with grayscale IVUS data, VH-IVUS regards the shadow region and other regions in a similar way.[12] Shadow regions usually occur behind DC regions without providing useful information for plaque characterization. Nevertheless, VH-IVUS classifies acoustic shadow regions as FFT or NC class, although they should be assigned as NC or DC.[13,14] Therefore, VH-IVUS results may differ from histology interpretations by pathologists for the shadow area.[13,14]

On the other hand, the amount of DC plaque accumulated in the arterial wall can be considered as an accurate indicator of atherosclerotic disease.[6] It is well known that the degree of calcification correlates with the overall risk of acute myocardial infarction. Therefore, if the shape and position of the calcified plaque and acoustic shadow are properly characterized, it will help physicians choose the appropriate treatment in order to reduce the risk of operation. However, most of the previously reported techniques have looked into the segmentation of inner and outer vessel borders. Only a few studies have attempted to characterize DC and acoustic shadow regions simultaneously from sequential IVUS image frames.[6,12,15]

Therefore, the purpose of this study was to use a dual-threshold-based segmentation approach to automatically detect DC and acoustic shadow regions in IVUS images. For this purpose, a total of three hundred IVUS and corresponding VH-IVUS images were acquired from 26 cardiovascular patients. DC and acoustic shadow regions were identified using the dual-threshold-based segmentation approach. To determine the reliability of the proposed method, four evaluation indexes were calculated along with ground truth data (VH-IVUS). The remainder of this manuscript is organized as follows. Details of the segmentation approach and performance evaluation are presented in Sect. 2. Experimental results and discussions are provided in Sects. 3 and 4, respectively. Finally, Sect. 5 concludes the paper and identifies future works.

2. Materials and Methods

DC and acoustic shadow were detected only for plaque regions of the original IVUS image. Plaque regions were manually accomplished by an expert for all IVUS images. They were

classified into FT, FFT, NC, or DC using VH-IVUS. The proposed approach detected DC tissue from IVUS images through a process consisting of coordinate conversion, noise removal, DC candidate extraction, and shadow detection. VH-IVUS was utilized as the ground truth to validate the segmentation performance of the proposed method. Experimental results were quantitatively assessed using various evaluation parameters. The process used for the detection of DC and corresponding acoustic shadow regions is shown in Fig. 1.

2.1 Image acquisition

Three hundred grayscale IVUS images and corresponding VH-IVUS images of right coronary arteries of 26 patients with known or suspected coronary artery disease were obtained. IVUS images with adequate involvements of FT, FFT, NC, and DC in plaque regions were selected as experimental subjects. Those images having no acoustic shadow were excluded. IVUS imaging was performed using a commercially available 20 MHz IVUS catheter (Eagle Eye, Volcano Therapeutics Inc., Rancho Cordova, CA, USA) with an imaging system. IVUS images were recorded and digitized along with a simultaneous ECG at 400 × 400 pixels in 8-bit grayscale. A motorized pullback was performed along the entire vessel at a speed of 0.5 mm/s, acquiring 30 frames/s using a dedicated pullback device. Written informed consent was obtained from all patients. The present study was approved by the Institutional Review Board of Ulsan University Hospital, Republic of Korea. For all IVUS image frames, intima and media-adventitial (MA) borders, also known as plaque regions, were manually segmented by an expert.

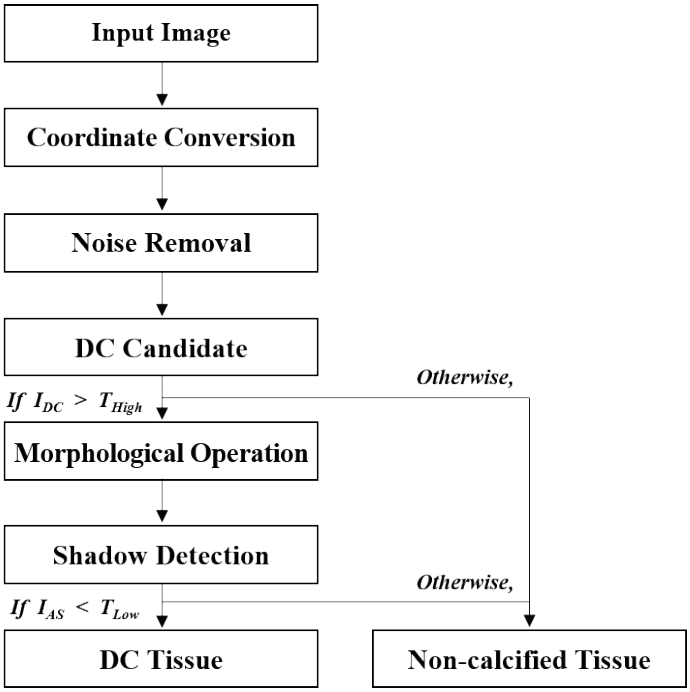

Fig. 1. Overall flowchart of the proposed approach for detecting DC and corresponding acoustic shadow from IVUS images (DC: dense calcium, I_{DC}: intensity of dense calcium, I_{AS}: intensity of acoustic shadow, T_{High}: high threshold, T_{Low}: low threshold).

2.2 Automated DC and acoustic shadow segmentation algorithm

The dual-threshold-based segmentation approach was used to segment DC and corresponding acoustic shadow regions in IVUS images. This method could detect DC and shadow regions using two thresholds. One was for detecting high-intensity regions that might belong to DC. The other was for identifying low-intensity regions (shadow region).

Owing to the circular trait of vessels, original IVUS images in Cartesian coordinates [Fig. 2(a)] were first converted into polar coordinates in order to simplify the segmentation steps [Fig. 2(b)]. Some parts of the image in IVUS frames such as calibration marks and scale marks were not significant for segmentation. In particular, the catheter created a dead zone at the center of the Cartesian domain, equivalently at top rows of the polar domain, along with imaging artifacts (Fig. 2). These artifacts should be removed. Otherwise, they will disrupt the detection process. The most straightforward approach to remove the dead zone is by subtracting the clear artifact zone from every frame. This does not degrade the image quality. However, it is not easy to obtain a constant artifact zone because the luminal border often interferes with the artifact zone. To avoid this limitation, the constant dead zone was extracted from the polar domain by calculating the minimum image $I_{min}(x,y) = \min_{i\in\lambda} I_i(x,y)$ over a set of frames (I_i) with IVUS sequence $\lambda^{(4)}$ (50 frames) [Fig. 2(c)]. The obtained constant artifact zone was then subtracted from every frame to avoid interference with the catheter as shown in Fig. 2(d). DC candidates were then acquired by extracting regions with a pixel intensity higher than T_{High} in lesion regions [Fig. 3(a)] as follows:

$$X_{DCC}(i,j) = \sum\left\{\left(I(i,j) > T_{High}\right)\right\} \in \mathrm{ROI}, \tag{1}$$

where X_{DCC} and $I(i,j)$ are the DC candidate region and the intensity of the pixel (i,j), respectively, and T_{High} is the high threshold for detecting the DC candidate. ROI is the region

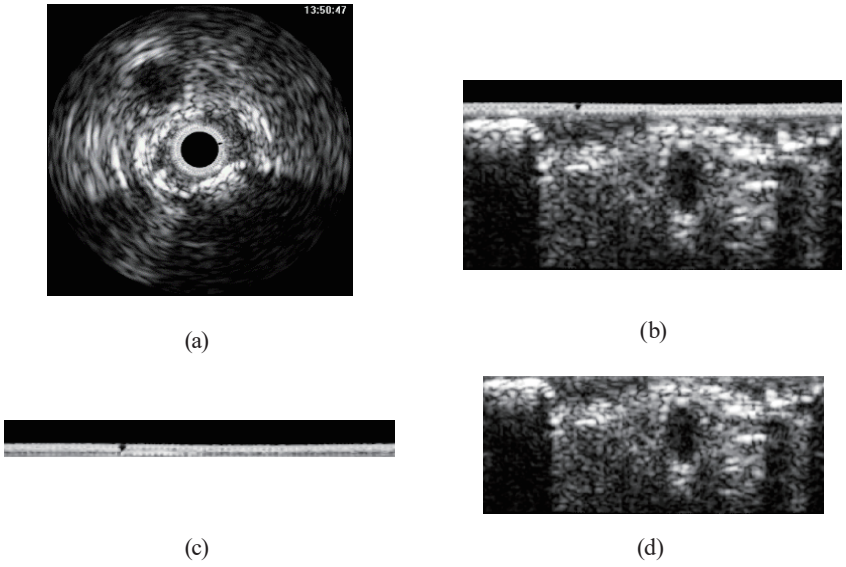

Fig. 2. Transformation of Cartesian to polar coordinates and removal of the dead zone based on the constant artifact zone (a) Cartesian coordinate, (b) polar coordinate, (c) constant artifact zone, and (d) catheter removed image.

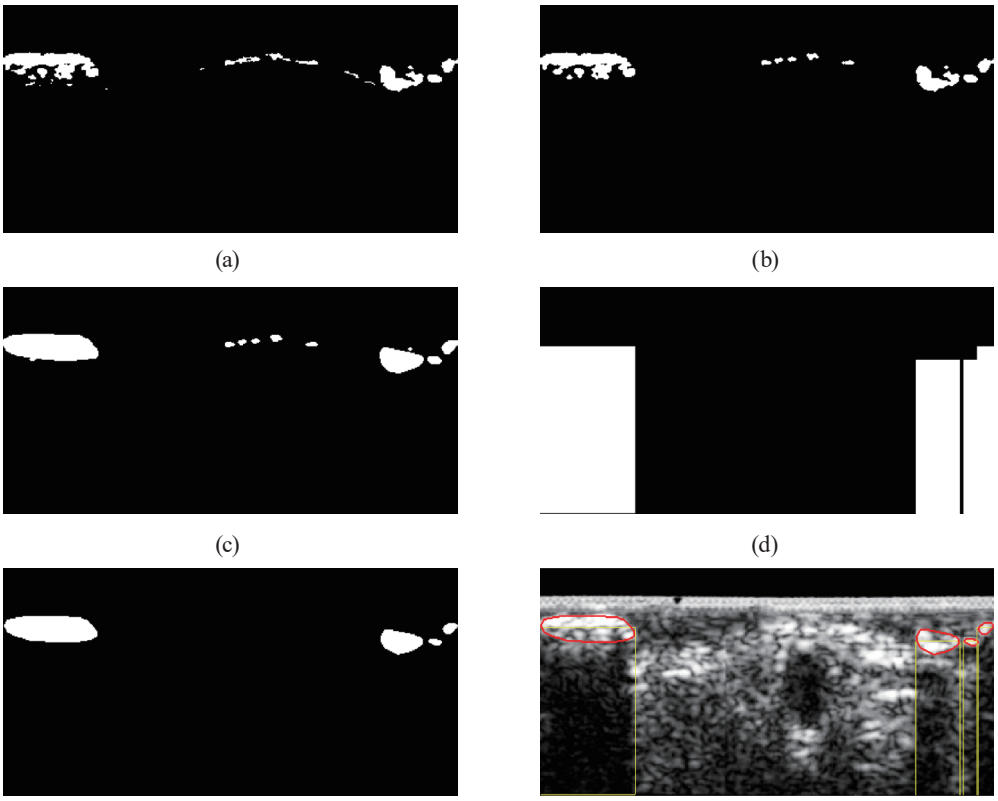

Fig. 3. (Color online) One example of the proposed method for detecting DC and corresponding acoustic shadow regions including (a) the detection of DC candidates, (b) morphological operation, (c) convex hull, (d) image mask of the acoustic shadow, (e) finally obtained DC tissue, and (f) superimposition of DC and shadow regions.

of interest (plaque region) and $\sum$ indicates the ensemble of the pixel. Morphological operation consisting of erosion and dilation was successively employed to remove unnecessary noises in the original image [Fig. 3(b)]. During morphological processing, the operation had a disk shape at a size of 1 × 1 pixel. The detected DC candidate regions often distributed very closely owing to inherent tissue characteristics. To minimize the computational load, these regions were merged as one by calculating the convex hull [16] when the distance of the adjacent DC candidate was less than 10 pixels [Fig. 3(c)].

DC candidate regions were classified into calcified or noncalcified groups according to the existence of acoustic shadow. To evaluate the presence of shadow, the centroid (center of mass) of each DC candidate was calculated. An image mask was generated by extracting the minimum and maximum locations of the y-axis following Eq. (2) [Fig. 3(d)].

$$M = \sum \left\{ X_{DCC}\left(i_{com}, \min(j)\right), X_{DCC}\left(i_{com}, \max(j)\right) \right\}, \tag{2}$$

where M is the outermost pixel coordinate of the shadow mask and i_{com} is the x-axis coordinate of the centroid. After mask extraction, the average of the local intensity placed in the same

angle as the DC candidate region was computed to evaluate the presence of shadow. For pixels that satisfied $I_{AS} < T_{Low}$, corresponding DC candidates were finally accepted to be in DC class [Fig. 3(e)]. Otherwise, they were regarded as noncalcified.

$$X_{DC}(i,j) = \sum \left\{ \left(I_{DCC}(i,j) > T_{High} \right) \text{and} \left(I_{AS}(i,j) < T_{Low} \right) \right\} \in \text{ROI}, \tag{3}$$

where X_{DC} is the detected calcified region and I_{DCC} and I_{AS} are the intensities of the DC candidate and shadow regions, respectively. In other words, only the region that satisfied both $I_{DCC} > T_{High}$ and $I_{AS} < T_{Low}$ was selected to be in the DC group. Threshold values for I_{DC} and I_{AS} were set at 160 and 50, respectively. These values were empirically obtained by determining the mean intensity of the DC and shadow regions in 300 IVUS images. Figure 3(f) demonstrates the superimposed DC estimates with the corresponding acoustic shadow.

Regarding computational load, the proposed method needed about 3.2 s to segment DC and the acoustic shadow in one IVUS image using an Intel(R) Core™ i7-2600 CPU at 3.40 GHz with 8.00 GB ram. All the parameters were maintained under the same condition during the detection procedure. All the procedures were implemented with MATLAB software package (R2015b, MathWorks Inc., Natick, MA, USA).

2.3 Performance validation

To quantify the detection performance, area difference (AD), DC ratio (DCR), Hausdorff distance (HD), and Dice similarity coefficient (DSC) between the proposed method and VH-IVUS were determined. AD is the mean area difference of the DC region. DCR is the corresponding ratio of DC regions between the proposed method and VH-IVUS. HD represented the similarity of the worst case fitting condition. It was defined as the maximum distance of the nearest pixel between two boundaries.[17,18] HD directly depicted pixel-to-pixel variation. It was calculated on the basis of the largest distance between pixels using the equation

$$HD(A,B) = \max \left\{ \max_{a \in A} \left(\min_{b \in B} |a-b| \right), \max_{b \in B} \left(\min_{a \in A} |a-b| \right) \right\}, \tag{4}$$

where $HD(A,B)$ is the HD between the detected boundaries A and B; $A = \{a_1, a_2, \ldots, a_n\}$ and $B = \{b_1, b_2, \ldots, b_n\}$.[19] For the coefficient ranging from 0 to 1, a value of 1 indicated perfect agreement, whereas a value of 0 indicated the absence of agreement.

DSC has been used as assessment metrics to measure the overlap between two regions.[19] It has been widely employed in the evaluation of medical image segmentation. DSC can be computed as

$$DSC(A,B) = \frac{2 \cdot |A \cap B|}{|A| + |B|}, \tag{5}$$

where $DSC(A,B)$ is the DSC between segmented DC regions obtained by the proposed method and VH-IVUS. If DSC had a value of 1, regions A and B had the same location and area.

3. Experimental Results

3.1 Comparing detection accuracy of DC region between the proposed method and VH-IVUS

Results of parameters including area, AD, DCR, HD, and DSC obtained by the proposed method and VH-IVUS are summarized in Table 1. The mean area difference of the DC region was 12.246 mm, which was relatively small. A relatively high similarity between the proposed method and VH-IVUS was found, with HD and DSC values of 0.540 and 0.596, respectively. On the other hand, some differences existed between the two approaches as shown in Fig. 4. DCR representing the mean overlapping ratio of DC regions was found to be 64.08%. Segmentation results of the DC region detected by the proposed method and VH-IVUS are shown in Fig. 5.

Table 1
Comparison of the evaluation parameters including AD, DCR, HD, and DSC between the proposed method and VH-IVUS.

ID	AD (mm)	DCR	HD	DSC
1	13.203	63.629	0.920	0.576
2	8.427	66.886	0.442	0.621
3	18.846	74.654	0.430	0.564
4	18.253	65.904	0.418	0.565
5	16.977	59.042	0.953	0.602
6	4.527	59.535	0.368	0.596
7	4.167	65.120	0.372	0.589
8	16.111	67.714	0.631	0.600
9	15.295	48.723	0.395	0.546
10	2.890	60.846	0.207	0.537
11	14.455	73.114	0.394	0.597
12	31.945	66.290	0.484	0.725
13	0.191	61.626	0.803	0.567
14	8.750	63.989	0.382	0.564
15	13.045	58.588	0.711	0.600
16	10.833	67.140	0.455	0.614
17	18.525	59.936	0.751	0.538
18	9.345	69.437	0.698	0.706
19	17.623	69.270	0.603	0.609
20	1.517	60.103	0.382	0.598
Mean	12.246	64.077	0.540	0.596

*AD: average difference, DCR: dense calcium ratio, HD: Hausdorff distance, DSC: Dice similarity coefficient.

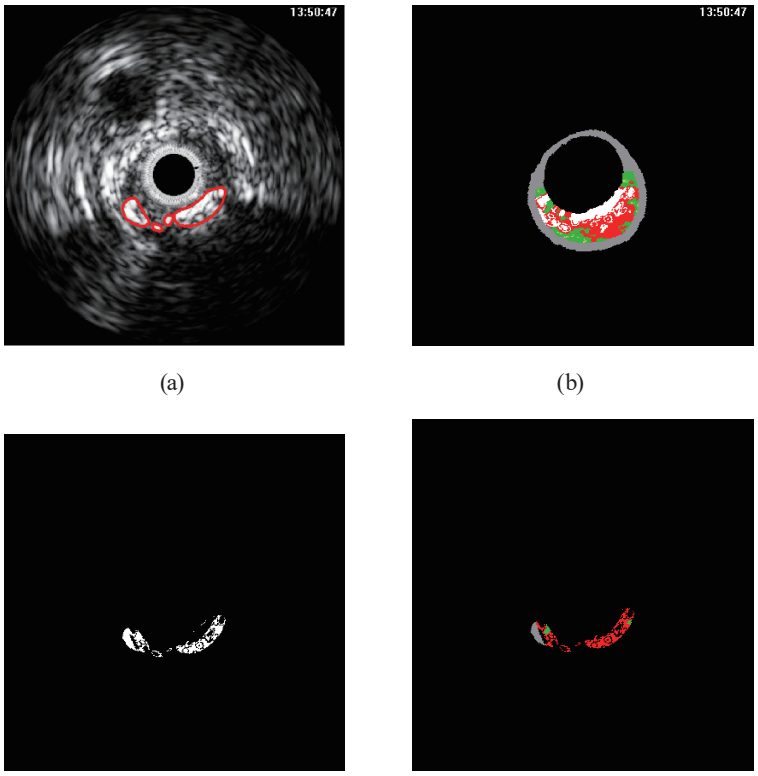

Fig. 4. (Color online) Comparison of the segmentation results of DC tissue: (a) proposed method and (b) VH-IVUS. (c) Differences between the proposed method and VH-IVUS. (d) Tissue characterization of (c).

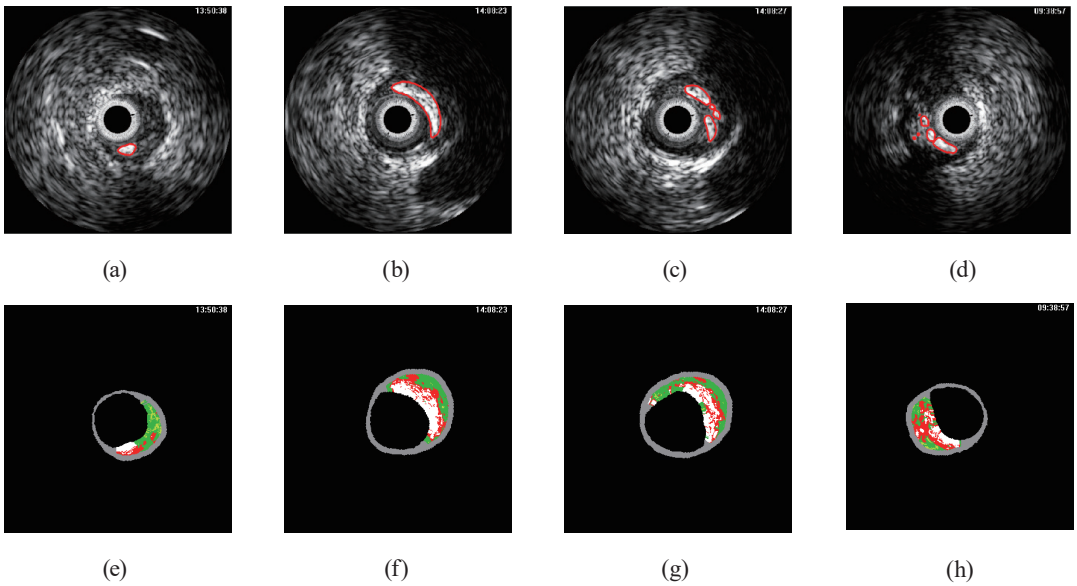

Fig. 5. (Color online) Segmentation results between the proposed method and VH-IVUS.

3.2 Tissue distribution for DC regions obtained by the proposed method

As mentioned above, DC regions obtained by the proposed method corresponded to approximately 64.08% compared with those by VH-IVUS. This indicated that the rest (35.92%) of the DC regions were classified into different tissues, such as FT, FFT, and NC. The analysis of the tissue distribution for these regions revealed that NC had the highest percentage (28.43%) as shown in Table 2, whereas FT and FFT occupied only 4.41 and 0.01%, respectively [Fig. 4(d)]. These experimental results revealed that the proposed approach had reliable segmentation performance despite the presence of some differences in the detected DC regions between the two methods.

4. Discussion

The performance of the proposed method for detecting DC and the corresponding acoustic shadow regions can be accurately evaluated by comparison with the arterial tissue distribution histologically. However, it is a very difficult and time-consuming process. VH-IVUS is a good alternative because of its fast and accurate tissue characterization. VH-IVUS classifies cardiovascular tissues into FT, FFT, NC, or DC based on reflected RF signals. Previous studies have reported that VH-IVUS is a reliable classification method with an accuracy above 93.5%.[20] Therefore, VH-IVUS was selected as the ground truth (reference) in this study to assess the segmentation performance of the proposed method. The intima and MA borders for tissue characterization were designated by experts for all IVUS images.

The analysis of DC detection between the proposed method and VH-IVUS showed reliable HD and DSC values for both groups. This is mainly because automatically detected DC regions by the proposed method and VH-IVUS showed similar distribution patterns as depicted in Fig. 5. The proposed method showed an agreement rate of 64.08% with VH-IVUS. To improve computational efficiency, DC candidates with a small distance of less than 10 pixels with neighboring candidates were used to compute convex hull [Fig. 3(c)]. However, considering that the remaining region except for DC class was mostly classified as NC tissue, this might be a controversial issue. Typically, the distribution of NC and DC tissues is regarded as one of the most important assessment factors for diagnosing cardiovascular diseases in IVUS images. However, the plaque region does not involve a relatively large amount of DC tissue with acoustic shadow in comparison with the entire image. In addition, NC tissues existing between detected DC regions play no significant role during lesion diagnosis because they are only distributed marginally. Obviously, these regions can also be partly detected on the basis of the existence

Table 2
Analysis of tissue distribution for the regions classified as different tissues, namely, FT, FFT, NC, and DC.

	FT (%)	FFT (%)	NC (%)	DC (%)
Proportion	4.41	0.01	28.43	64.08

*FT: fibrous tissue, FFT: fibro-fatty tissue, NC: necrotic core, DC: dense calcium.

of acoustic shadow. However, this study focused on the optimization of computational load rather than the accurate segmentation of DC. Another reason for this result comes from the DC distribution on VH-IVUS. The calcified area usually involves a corresponding lateral shadow region. However, some regions were classified as DC class, although there was no shadow behind them. These factors might have affected the agreement between the proposed method and VH-IVUS.

The rest of the automatically detected DC regions by the proposed method but not by VH-IVUS were mostly classified as NC, while FT and FFT accounted for only 4.41 and 0.01%, respectively. Interestingly, FFT has a very low percentage. This might be due to the detection characteristic of the proposed method for DC and acoustic shadow. Typically, the mean intensities of arterial tissues are in the order of DC > NC > FT > FFT in IVUS sequences.[15,21] Moreover, the overlapping region between FFT and DC is quite small because these tissues have quite different intensity profiles. Existing approaches have attempted to classify tissue compositions on the basis of these characteristics and verified that the intensity could be a good indicator for tissue characterization.[15,21] The proposed method implemented dual threshold in order to detect DC and the corresponding acoustic shadow in IVUS images. For this purpose, most FT and FFT with relatively low intensities were excluded through the criterion of $I > T_{High}$. Only the regions that satisfied the condition $I < T_{Low}$ were finally selected as DC. This might have caused the very small distributions of FT and FFT.

The major contribution of this study is that it is possible to segment DC and acoustic shadow regions reliably using only intensity information in comparison with VH-IVUS, which utilizes tricky and complex RF signals. Another obvious advantage of the proposed method is that it can automatically detect DC and shadow from IVUS images. This can help clinicians diagnose various cardiovascular diseases. According to the distribution and location of detected DC, clinicians will be able to establish appropriate treatment strategies. Moreover, the proposed method can be easily implemented to image-based tissue characterization techniques to improve the diagnostic accuracy and efficiency of existing methods.

One of the main limitations of this study was that VH-IVUS data were designated as the ground truth for assessing the segmentation performance of the proposed method. Although VH-IVUS imaging provides acceptable correlation with histologic analyses, even a subtle error in VH-IVUS can affect the entire procedure, thus influencing the agreement between the proposed method and VH-IVUS. VH-IVUS can be utilized as a basis for validating segmentation performance. However, it should not be considered as the ground truth. Another limitation of this method was that NC, which was regarded as DC during the segmentation process, was not properly extracted because the proposed method focused on the optimization of computational load. This region cannot be easily differentiated using only the intensity characteristic. Additional texture features are needed. To solve these limitations, further study is needed to improve the segmentation performance for DC and acoustic shadow. In addition, a convolutional neural-network-based classification model needs to be developed to characterize cardiovascular tissue components. We also needed to directly evaluate the segmentation performance of the proposed method via histologic analysis.

5. Conclusions

In this study, we automatically segmented DC and corresponding acoustic shadow regions based on dual threshold from IVUS image sequences. The performance of the proposed method was evaluated by evaluating parameters such as AD, DCR, HD, and DSC. Quantitative analyses indicated that the proposed method had reliable segmentation performance compared with VH-IVUS. In particular, the proposed method showed high similarity with VH-IVUS despite a relatively low agreement rate. Moreover, DC regions detected by the proposed approach involved only small amounts of FT and FFT. These experimental results suggest that the proposed method has clinical applicability for the diagnosis of cardiovascular diseases based on IVUS images. To improve its segmentation performance, further study is needed using various vessel conditions.

Acknowledgments

This work was supported by the International Collaborative R&D Program (N0000684) funded by the Ministry of Trade, Industry & Energy (MOTIE), Korea [N01150049, developing high frequency bandwidth (40–60 MHz) high-resolution image system and probe technology for diagnosing cardiovascular lesion].

References

1 G. K. Hansson: N. Engl. J. Med. **21** (2005) 1685.
2 P. C. Choy, Y. L. Siow, D. Mymin, and K. O: Biochem. Cell Biol. **82** (2004) 212.
3 E. Falk: J. Am. Coll. Cardiol. **18** (2006) C7.
4 G. Unal, S. Bucher, S. Carlier, G. Slabaugh, T. Fang, and K. Tanaka: IEEE Trans. Inf. Technol. Biomed. **12** (2008) 335.
5 D. G. Vince, K. J. Dixon, R. M. Cothren, and J. F. Cornhill: Comput. Med. Imaging Graph. **24** (2000) 221.
6 A. Taki, Z. Najafi, A. Roodaki, S. K. Setarehdan, R. A. Zoroofi, A. Konig, and N. Navab: Int. J. Comput. Assist. Radiol. Surg. **3** (2008) 347.
7 E. G. Mendizabal-ruiz, M. Rivera, and I. A. Kakadiaris: Med. Image Anal. **17** (2013) 649.
8 M. Valgimigli, P. Agostoni, and P. W. Serruys: J. Cardiovasc. Med. **8** (2007) 221.
9 A. Mantziari, A. Ziakas, G. Stavropoulos, and I. H. Styliadis: Hippokratia **15** (2011) 60.
10 A. Nair, M. P. Margolis, B. D. Kuban, and D. G. Vince: EuroIntervention **3** (2007) 113.
11 A. Nair, B. D. Kuban, E. M. Tuzcu, P. Schoenhagen, S. E. Nissen, and D. G. Vince: Circulation **22** (2002) 2200.
12 A. Taki, A. Roodaki, S. K. Setarehdan, S. Avansari, G. Unal, and N. Navab: Comput. Biol. Med. **43** (2013) 268.
13 G. S. Mintz, H. M. Garcia-Garcia, S. J. Nicholls, N. J. Weissman, N. Bruining, T. Crowe, J. C. Tardif, and P. W. Serruys: EuroIntervention **6** (2011) 1123.
14 N. Bruining, S. Verheye, M. Knaapen, P. Somers, J. R. Roelandt, E. Regar, I. Heller, S. de Winter, J. Ligthart, G. Van Langenhove, P. J. de Feijter, P. W. Serruys, and R. Hamers: Catheter Cardiovasc. Interv. **70** (2007) 968.
15 A. Taki, H. Hetterich, A. Roodaki, S. K. Setarehdan, G. Unal, J. Rieber, N. Navab, and A. König: Ultrasound Med. Biol. **36** (2010) 1245.
16 F. P. Preparata and M. I. Shamos: Computational Geometry: An Introduction (Springer-Verlag, New York, 1998).
17 D. P. Huttenlocher, G. A. Klanderman, and W. J. Rucklidge: IEEE T. Pattern Anal. **15** (1993) 850.
18 V. Chalana and Y. Kim: IEEE T. Med. Imaging **16** (1997) 642.
19 X. Qin, Z. Cong, and B. Fei: Phys. Med. Biol. **58** (2013) 7609.
20 A. Nair, M. P. Margolis, B. D. Kuban, and D. G. Vince: EuroIntervention **3** (2007) 113.
21 L. S. Athanasiou, P. S. Karvelis, V. D. Tsakanikas, K. K. Naka, L. K. Michalis, C. V. Bourantas, and D. I. Fotiadis: IEEE T. Inf. Technol. Biomed. **16** (2012) 391.

About the Authors

Ju Hwan Lee was born in Seoul, Korea, in 1983. He received his B.S. degree in Biomedical Engineering from Konkuk University, Korea, in 2009, and his M.S. degree in Medical Biotechnology from Dongguk University, Korea, in 2010. He also received his Ph.D. degree in Medical Biotechnology from the same university in 2015. Since 2015, he has been a research professor in the Department of Medical Devices Industry, Dongguk University, Korea. He is the author of more than 40 articles and 5 patents. His research interests include medical image analysis, image segmentation, and pattern recognition.

Ga Young Kim was born in Seoul, Korea, in 1993. She received her B.S. degree in Medical Biotechnology from Dongguk University, Korea, in 2015 and her M.S. degree from the same university in 2016. Since 2016, she has been a Ph.D. candidate in the Department of Medical Biotechnology of the same university. Her research interests include medical image analysis, neural network, and pattern recognition.

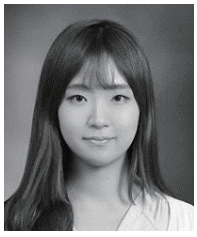

Yoo Na Hwang was born in Seoul, Korea, in 1990. She received her B.S. degree in Electronic Engineering from Dongguk University, Korea in 2014, and her M. S. degree from the Department of Medical Devices Industry of the same university in 2016. Since 2016, she has been a Ph.D. candidate in the Department of Medical Biotechnology of the same university. Her research interests include medical image analysis, neural network, and pattern recognition.

Sung Min Kim was born in Seoul, Korea, in 1962. He received his B.S. degree in Electrical Engineering from Yonsei University, Korea, in 1985, and his M.S. degree in Biomedical Engineering from the University of Iowa, in 1991. He received his Ph.D. degree in Biomedical Engineering also from same university in 1995. From 2002 to 2009, he was an associate professor in the Department of Biomedical Engineering, Konkuk University, Korea. Since 2009, he has been a professor in the Department of Medical Biotechnology, Dongguk University, Korea. He is the author of five books, more than 120 articles, and more than 70 patents. His research interests include medical image processing, signal processing, biomedical modeling, tissue engineering, biomaterial engineering, and biomechanics.